# Communication

## Endfire Antenna Array Using Microstrip-Fed Cavity-Backed Slot Elements

Yuefeng Hou, Zhijun Meng, Lifeng Wang, and Yue Li

***Abstract*— In this communication, an endfire antenna array using series-fed cavity-backed slot elements is proposed with low profile and high gain properties. By adopting the cavity-backed slot element as the radiating element, the antenna array can be partly embedded under the ground plane, which reduces the profile. Fed by an air–substrate microstrip line, the antenna array achieves a moderate phase constant, which leads to an endfire radiation pattern. By optimizing the coupling level between the cavity-backed slot elements and microstrip line, the aperture distribution of the antenna array is improved to enhance the endfire gain. With the overall length of 3.75 wavelength at 4 GHz, the proposed antenna array obtains a measured endfire gain of 11.5 dBi. Compared with the low-profile endfire antennas mounted on the metallic plane, the proposed antenna array has lower profile and higher endfire gain.**

***Index Terms*— Cavity-backed slot, endfire, high gain, low profile, series fed.**

### I. Introduction

The antennas with endfire radiation mounted on a metallic plane have been developed for the demand of the missile and unmanned aerial vehicle positioning systems. To increase the communication distance and decrease the aerodynamic drag, the characteristics of low profile and high endfire gain are important for such type of antennas. However, it is still a challenge for the antennas mounted on a metallic plane to achieve the properties of low profile and high endfire gain simultaneously. In the open literatures and textbooks, most of the antennas have relatively small radiating apertures or nonuniform aperture distributions, which limit the antennas to realize a high endfire gain. For example, for the log-periodic antennas in [1]–[3] and surface wave antennas in [4] and [5] with a broad bandwidth, only partial radiating apertures are used at a desired operating frequency. Because of the relatively small dimension of the radiating aperture, the horn antenna in [6] is with a sloping-upward beam. For the Yagi antennas in [7]–[9], the increase in the director element number has a weaker influence on the endfire gain when the element number becomes larger. Thus, the aforementioned antennas are with relatively low gain at the endfire direction.

To obtain a high gain on the endfire direction, the series-fed antenna array is a feasible solution to ease realization of a large radiating aperture, which can be achieved by adjusting the coupling level between the radiating elements and the feed structure. For the endfire antennas in [10] and [11], they are fed by a substrate integrated waveguide operating on $TE_{10}$ mode. However, because $TE_{10}$ mode is a dispersive mode, the beam directions of the antennas in [10] and [11] drastically change versus frequency. To achieve a stable endfire radiation pattern, the air–substrate microstrip line is a good candidate as the feeding line of the endfire antenna, because it works on non-dispersive TEM mode, which has the phase constant satisfying the requirement of the endfire radiation. The air–substrate microstrip feeding line has already been adopted in several designs [12]–[15]. Nevertheless, for the designs in [12] and [13], the profiles of the antennas are too high, which are close to a quarter of wavelength at the center frequency. For the low-profile designs in [14] and [15], they might have high fabrication complexity. Furthermore, due to the low-profile configuration, the quality factors of the radiating elements in [14] and [15] are relatively large, which reduces the gain bandwidth of the antenna.

In this communication, an endfire antenna array with low profile and high gain is designed. The radiating elements of the antenna array, which are cavity-backed slot elements, are series-fed by an air–substrate microstrip line, leading to a long radiating aperture and a moderate phase constant. By optimizing the coupling level between the cavity-backed slot elements and microstrip line, the aperture distribution of the antenna array is improved. Surrounded by metal sides, the cavity-backed slot elements can be embedded under the ground plane. With the designed merits of large radiating aperture length, moderate phase constant, uniform aperture distribution, and partly embedded structure, the proposed antenna array has a lower profile and a higher endfire gain compared with the ones for the same purpose. To verify the design strategy, a prototype with the length of 3.75 $\lambda_0$ and the profile of 0.013 $\lambda_0$ is built and fabricated. $\lambda_0$ is the free-pace wavelength at the center frequency of 4 GHz. The measured results show that the antenna array can obtain the high endfire gain of 11.5 dBi and the moderate 3 dB gain bandwidth of 17.7%.

TABLE I
Detailed Dimension of the Antenna Array

| Parameter | Value (mm) | Parameter | Value (mm) |
|---|---|---|---|
| $M_L$ | 281.25 | $C_P$ | 18.75 |
| $M_W$ | 5 | $C_W$ | 59 |
| $M_H$ | 1 | $C_H$ | 8 |
| $M_T$ | 3.5 | $G_L$ | 356.25 |
| $S_W$ | 8 | $G_W$ | 134 |

### II. Element Design Consideration

The radiating element of the antenna array is a cavity-backed slot element, which can be embedded under the ground plane, as illustrated in Fig. 1. The cavity-backed slot element consists of an air-filled metallic cavity and a ground plane notched by a slot. The detailed dimension of the cavity-backed slot element is presented in Table I.

The lengths $C_W$ of the slot and cavity are the same with each other. According to (1) [16], the lowest resonant frequency of cavity is

Manuscript received November 7, 2018; revised August 12, 2019; accepted August 31, 2019. Date of publication September 16, 2019; date of current version March 3, 2020. This work was supported in part by the National Natural Science Foundation of China under Contract 61771280 and in part by the Beijing Natural Science Foundation under Contract 4182029. *(Corresponding authors: Zhijun Meng; Yue Li.)*

Y. Hou and Y. Li are with the Department of Electronic Engineering, Tsinghua University, Beijing 100084, China (e-mail: lyee@tsinghua.edu.cn).

Z. Meng and L. Wang are with the School of Aeronautic Science and Engineering, Beijing University of Aeronautics and Astronautics, Beijing 100191, China (e-mail: mengzhijun@buaa.edu.cn).

Color versions of one or more of the figures in this communication are available online at http://ieeexplore.ieee.org.

Digital Object Identifier 10.1109/TAP.2019.2940493

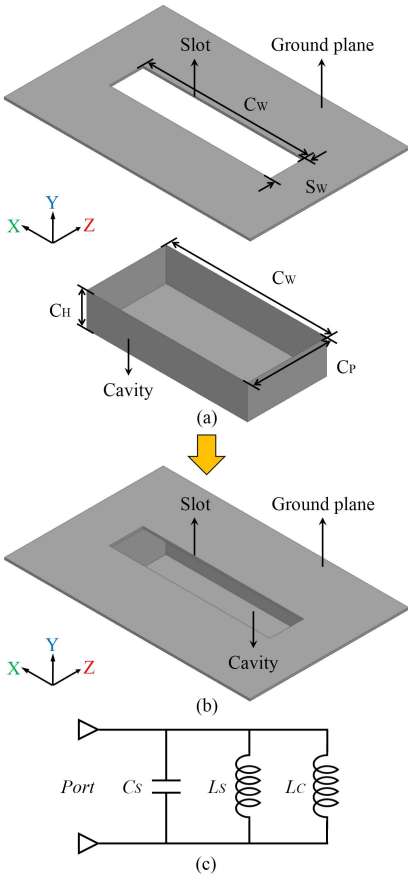


Fig. 1. Configuration and operating principle of the cavity-backed slot element. (a) Exploded view. (b) Perspective view. (c) Equivalent circuit model.

much higher than the center frequency of 4 GHz. Therefore, the non-resonant backed cavity is regarded as a reflector to restrict the slot radiating on the upper hemisphere

$$f_{101} = \frac{c}{2\pi\sqrt{\varepsilon_r \mu_r}}\sqrt{\left(\frac{\pi}{C_W}\right)^2 + \left(\frac{0}{C_H}\right)^2 + \left(\frac{\pi}{C_P}\right)^2}. \quad (1)$$

To clearly analyze the character of the cavity-backed slot element, a simplified circuit model is designed, as plotted in Fig. 1(c). The slot corresponds to a parallel resonant circuit which is composed of a capacitor $C_S$ and an inductor $L_S$. Because the height $C_H$ of the cavity is smaller than 0.25 $\lambda_0$, the backed cavity corresponds to a parallel inductor $L_C$. Based on the circuit model, the center frequency of the proposed cavity-backed slot is expressed as

$$f_0 = \frac{1}{2\pi\sqrt{\frac{L_S L_C}{L_S + L_C} C_S}}. \quad (2)$$

To energize the cavity-backed slot element, an air–substrate microstrip line is adopted as the feed structure. The microstrip line is formed by the copper strip and ground plane. On the ground plane, the electric current distribution is presented in Fig. 2. The electric current with the blue color is caused by the microstrip line, and the electric current with the purple color is excited by the cavity-backed slot element. From Fig. 2, on one side of the slot, the two electric currents flow along the same direction ($z$-axis). Because of the similar modal electric current field configurations around the edge of the slot, the cavity-backed slot element can be fed by the microstrip line.

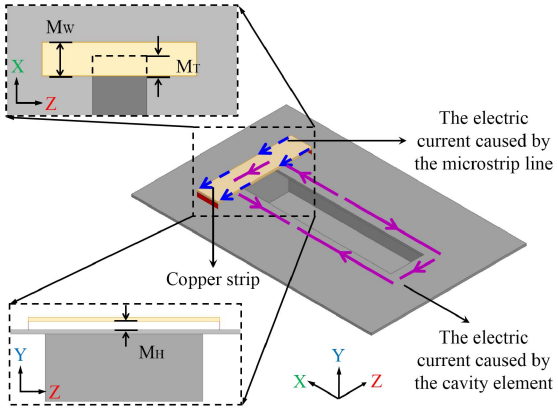


Fig. 2. Configuration and operating principle of the cavity-backed slot element fed by a microstrip line.

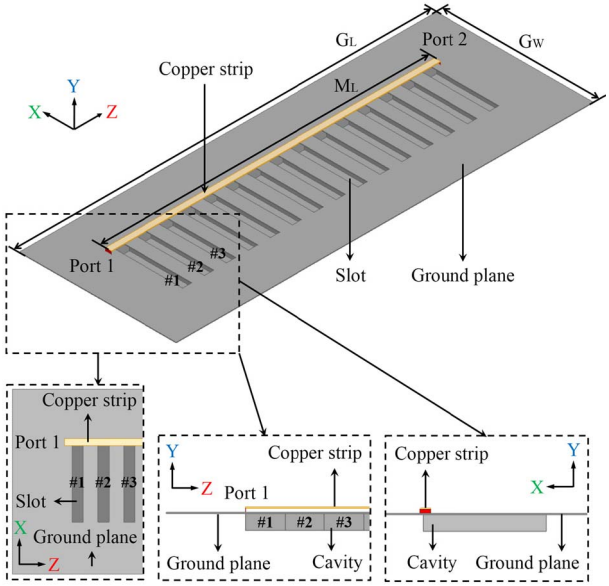


Fig. 3. Configuration of the antenna array using microstrip-fed cavity-backed slot elements.

## III. Antenna Design Consideration

By periodically arranging the 15 identical cavity-backed slot elements in a line and adopting an air–substrate microstrip line as the feed structure, the antenna array with a large radiating aperture is performed in Fig. 3. The dimensions of the antenna array are shown in Table I in detail.

When the cavity-backed slot elements are periodically placed along the microstrip line, the periodicity may introduce high-order space harmonics [17]. The beam direction $\theta_n$ of the $n$-order space harmonic can be calculated by

$$\theta_n = \cos^{-1}\left(\frac{\beta_n}{k_0}\right) \quad (3)$$

$$\beta_n = \beta_0 + \frac{2n\pi}{C_P} \quad (4)$$

where $\beta_n$ is the phase constant of the $n$-order space harmonic, $\beta_0$ is the phase constant in free space, and $k_0$ is the propagation constant in free space. To avoid exciting high-order space harmonics, the separation $C_P$ between the adjacent cavity-backed slot elements should be obviously smaller than 0.5 $\lambda_0$ [18]. To achieve a better matching performance, the distance is chosen as 0.25 $\lambda_0$ [14], [19].

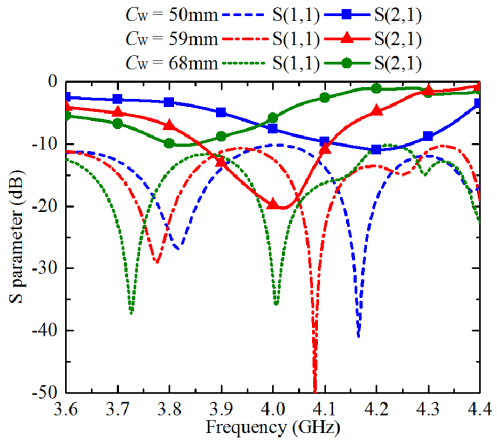


Fig. 4. Simulated S-parameters of the antenna array with different $C_W$.

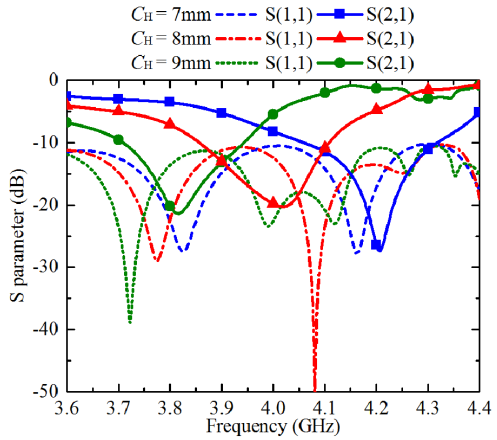


Fig. 5. Simulated S-parameters of the antenna array with different $C_H$.

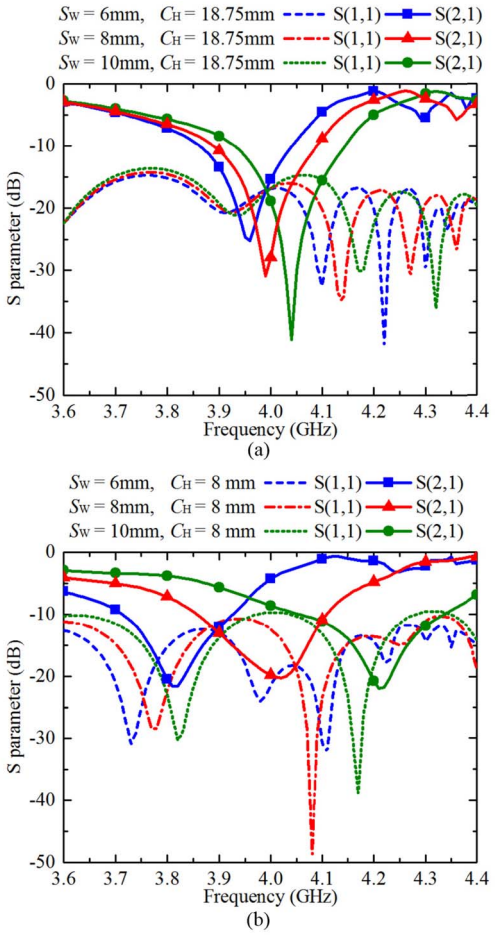


Fig. 6. Simulated S-parameters of the antenna array with different $S_W$, when (a) $C_H = 18.75$ mm (0.25 $\lambda_0$) and (b) $C_H = 8$ mm ($\approx 0.11$ $\lambda_0$).

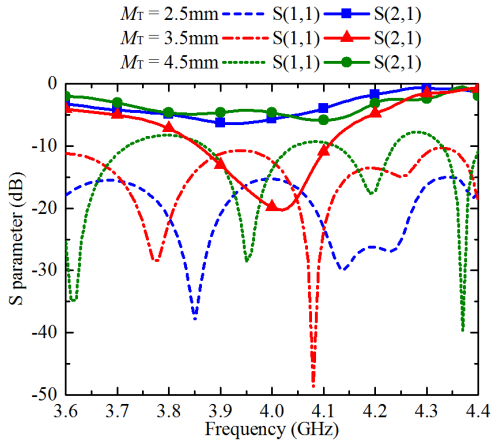


Fig. 7. Simulated S-parameters of the antenna array with different $M_T$.

The center frequency of the antenna array is defined as the frequency point where the transmission magnitude is the lowest. When the cavity-backed slot element is resonant, it can couple more energy from the microstrip line. Thus, the center frequency of the antenna array is mainly determined by the resonant frequency of the cavity-backed slot element.

Referring to the equivalent circuit model and (2), if the length $C_W$ of the slot raises, the values of the capacitor $C_S$ and inductor $L_S$ increase simultaneously, which would decrease the center frequency of the antenna array. As shown in Fig. 4, by adjusting the length $C_W$ of the slot from 50 to 68 mm, the center frequency of the antenna array changes from 4.21 to 3.83 GHz. If the height $C_H$ of the cavity raises from 0 to 0.25 $\lambda_0$, the value of the inductor $L_C$ increases from 0 to infinity, which would reduce the center frequency of the antenna array. As illustrated in Fig. 5, by adjusting the height $C_H$ of the cavity from 7 to 9 mm, the center frequency of the antenna array changes from 4.21 to 3.82 GHz. When the width $S_W$ of the slot raises, the value of the inductor $L_S$ increases, whereas the value of the capacitor $C_S$ decreases, which would reduce the quality factor and enhance the bandwidth. Based on (2), if the influence of the inductor $L_C$ can be neglected ($C_H = 0.25$ $\lambda_0$), the center frequency of the antenna array would be almost unchanged with a raising width $S_W$, otherwise, the center frequency would increase. As plotted in Fig. 6, by adjusting the width $S_W$ of the slot from 6 to 10 mm, the center frequency of the antenna array changes from 3.96 to 4.04 GHz when the height $C_H$ of the cavity is 0.25 $\lambda_0$, and the center frequency changes from 3.81 to 4.21 GHz when the height $C_H$ is 0.11 $\lambda_0$. Based on the investigation mentioned above, if the center frequency of the antenna array maintains unchanged, the height $C_H$ of the element can be reduced at the expense of increasing the length $C_W$ and decreasing the width $S_W$.

Keeping the other parameters unchanged, the coupling level between the microstrip line and cavity-backed slot element can be adjusted by modifying the overlap distance $M_T$. As depicted in Fig. 7,

TABLE II
PERFORMANCES OF THE ANTENNA ARRAY WITH DIFFERENT DIMENSIONS

| $C_H$ (mm) | $C_W$ (mm) | $M_T$ (mm) | Max. $\|S_{11}\|$ (dB) | $\|S_{12}\|$ (dB) | Dir. (dBi) | -3 dB Gain BW (%) |
|---|---|---|---|---|---|---|
| 8 | 59.0 | 3.5 | -10.3 | -19.9 | 12.1 | 15.0 |
| 10 | 46.5 | 3.0 | -11.9 | -16.5 | 12.1 | 13.9 |
| 12 | 42.5 | 2.5 | -13.3 | -32.6 | 12.1 | 13.2 |
| 14 | 40.0 | 2.3 | -13.7 | -27.4 | 12.1 | 12.6 |
| 16 | 38.5 | 2.0 | -14.2 | -21.6 | 12.0 | 12.2 |
| 18 | 37.5 | 2.0 | -14.1 | -23.1 | 12.0 | 11.8 |

when the distance $M_T$ is 3.5 mm, more energy in the microstrip line is coupled by the cavity-backed slot elements, leading to a lower transmission magnitude. From Fig. 7, influenced by the more serious discontinuity on the ground plane, the reflection magnitude of the microstrip line deteriorates when the overlap distance $M_T$ increases.

To achieve an endfire antenna array with high endfire gain, low height, reasonable reflection magnitude, and moderate gain bandwidth, a wide slot with the width $S_W$ of 8 mm is adopted, and the height $C_H$, length $C_W$, and overlap distance $M_T$ are optimized, as presented in Table II. The Max. $|S_{11}|$ is the maximum reflection magnitude from 3.6 to 4.4 GHz. From Table II, with the height $C_H$ decreasing and the length $C_W$ increasing, it is found that 1) the magnitude distribution on the slot changes to nonuniform, which leads to a nearly unchanged directivity; 2) the quality factor of the cavity-backed slot element reduces, which results in a wider $-3$ dB gain bandwidth; and 3) the electric current densities on the edges of the slot become lower, which causes a higher overlap distance $M_T$ and a worse reflection magnitude. As a compromise, the antenna array with the height $C_H$ of 8 mm is selected in this communication.

According to the above descriptions, the design procedure of the antenna array can be summarized as follows: 1) first, the width $M_W$ of the copper strip is adjusted to realize a microstrip line with low reflection magnitude. 2) Then, the width $S_W$ of the slot is adjusted to obtain a suitable gain bandwidth. 3) Next, the height $C_H$ and length $C_W$ of the cavity-backed slot element are modified to change the center frequency of the antenna array. 4) Finally, the distance $M_T$ is varied to achieve a high leakage constant around the center frequency.

## IV. PERFORMANCE ANALYSIS

To better evaluate the performance of the antenna array, the leakage constant $\alpha$, phase constant $\beta$, and aperture distribution are investigated. As exhibited in Fig. 8, the leakage constant $\alpha$ is frequency dependent because of the resonant feature of the cavity-backed slot elements. Around the center frequency, more energy in the microstrip line is coupled to the cavity-backed slot elements, achieving a higher leakage constant.

Although the feed structure of the antenna array, which is an air–substrate microstrip line, operates on the non-dispersive TEM mode, influenced by the loading of the cavity-backed slot elements, the phase constant $\beta$ of the antenna array is slightly higher than $k_0$. As a comparison, the normalized phase constants of the Hansen–Woodyard (H-W) condition [20], modified H-W condition [21], and proposed antenna array are shown together in Fig. 8. Both the H-W condition [20] and modified H-W condition [21] are the optimum conditions for maximizing directivity at endfire. However, the H-W condition [20] is applied in the antenna arrays with a constant aperture distribution, and the modified H-W condition [21] is suitable for the antenna array with an exponentially decaying aperture distribution, which is more practical in reality. From Fig. 8,

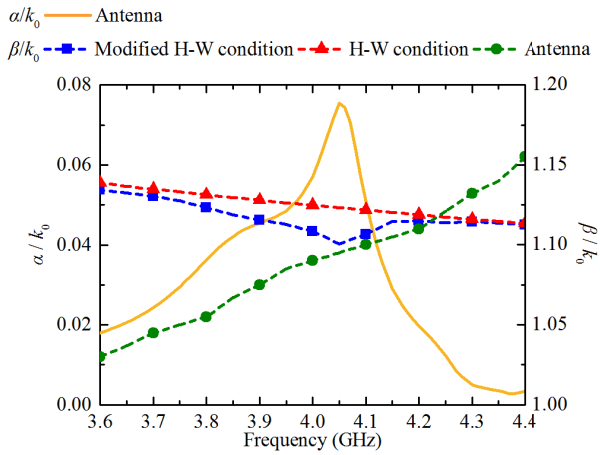


Fig. 8. Normalized leakage constant $\alpha/k_0$ and normalized phase constant $\beta/k_0$ of the antenna array versus frequency.

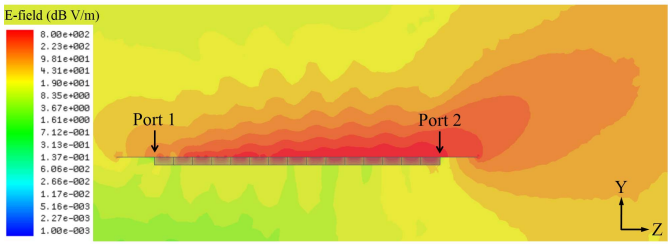


Fig. 9. The electric field magnitude distribution on the middle plane perpendicular to the radiating aperture at the center frequency of 4 GHz. The antenna array is excited at the Port 1, and the Port 2 is terminated with a matching load.

it is found that the phase constant $\beta$ of the antenna array is moderate and close to the phase constants of the modified H-W condition and H-W condition around the center frequency. Consequently, if the effect of the edge diffraction of the finite ground plane is neglected, the main beam direction of the antenna array is approximate to endfire from 3.6 to 4.4 GHz on the basis of (3), and a high endfire gain can be obtained by the antenna array at the center frequency of 4 GHz.

With a reasonable coupling level between the cavity-backed slot elements and microstrip line, the overall radiating aperture is effectively excited. Influenced by the cavity-backed slot elements, the electric current of the microstrip line on the ground plane is periodically interrupted, which energizes a leaky mode [10]. Nevertheless, because the phase constant $\beta$ of the antenna array is slightly higher than $k_0$, the energy of the leaky mode sharply attenuates on the radiating aperture, and the energy propagates with the surface-wave mode along the endfire direction [10], [22]. As shown in Fig. 9, because of the superposition of the leaky mode energy around the cavity-backed slot elements and the surface-wave mode energy propagating on the radiating aperture, the aperture distribution of the antenna array is relatively uniform, which is good for the endfire gain improvement.

## V. EXPERIMENTAL RESULTS

The fabricated prototype of the antenna array is presented in Fig. 10. The ground plane and copper strip of the antenna array are fabricated using 0.5 mm-thick copper plates. Two coaxial lines are connected to the two sides of the copper strip. To mitigate the effect of the discontinuities between the microstrip line and the coaxial lines, two isosceles trapezoid structures are added between them. One side of the isosceles trapezoid structure has the same width of 5 mm as

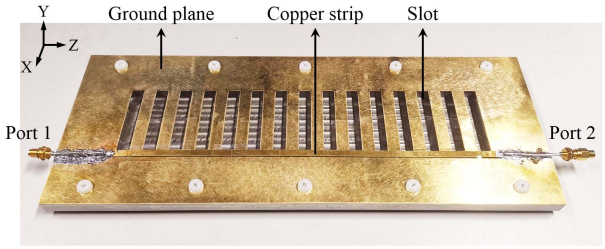


Fig. 10. Fabricated prototype of the antenna array.

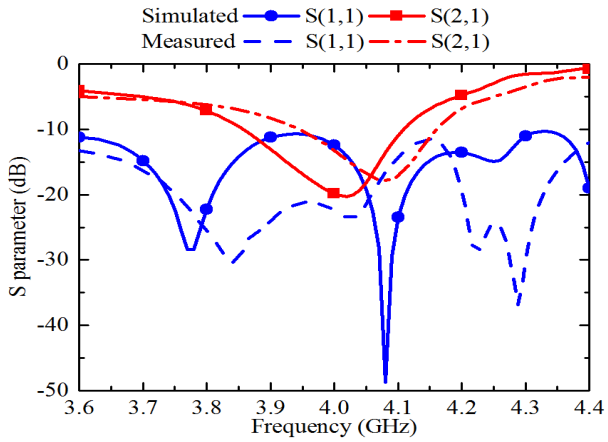


Fig. 11. Simulated and measured S-parameters of the antenna array.

the copper strip and the other side is 4 mm wide. The length of the isosceles trapezoid structure is 2 mm. In the assembly, the overlap distance $M_T$ is adjusted based on the S-parameters of the antenna array. Fabricating by the 0.5 mm-thick copper plate, the copper strip is light. A foam with the height of 1 mm is placed under the copper strip as the support. Hence, the copper strip and the foam can be fastened tightly on the ground plane with a wide tape.

The Port 1 of the antenna array is excited, and a matching load is connected to the Port 2. S-parameter was measured by a N5071B vector network analyzer (300 kHz to 9 GHz), and the gains and radiation patterns were measured in a far field anechoic chamber. As shown in Fig. 11, the simulated and measured reflection magnitudes are lower than −10 dB from 3.6 to 4.4 GHz. The simulated and measured transmission magnitudes are lower than −10 dB from 3.86 to 4.11 GHz and from 3.95 to 4.16 GHz, respectively. As exhibited in Fig. 12, the simulated endfire gain of the antenna array is higher than 10 dBi from 3.73 to 4.22 GHz with the maximum value of 12.1 dBi at 4.07 GHz. The measured endfire gain of the antenna array is higher than 10 dBi from 3.82 to 4.26 GHz with the maximum value of 11.8 dBi at 4.1 GHz. The simulated and measured front to back ratios are higher than 10.5 and 16.5 dB over the operating frequency bandwidth, respectively. The simulated 1 and 3 dB gain bandwidths are 8.3% and 15%, respectively. The measured 1 and 3 dB gain bandwidths are 9.1% and 17.7%, respectively.

The normalized radiation pattern of the antenna array on the *YOZ* plane is illustrated in Fig. 13(a). Influenced by the edge diffraction of the finite ground plane, the simulated and measured main beam directions are about 13° away from the endfire direction. The simulated and measured first sidelobe levels are about −3.1 dB. Referring to [11], [23], and [24], the sidelobe level can be reduced by optimizing the phase constant or aperture distribution. As presented in Fig. 13(b), the simulated and measured half-power beamwidths of the normalized radiation pattern on the *XOZ* plane are

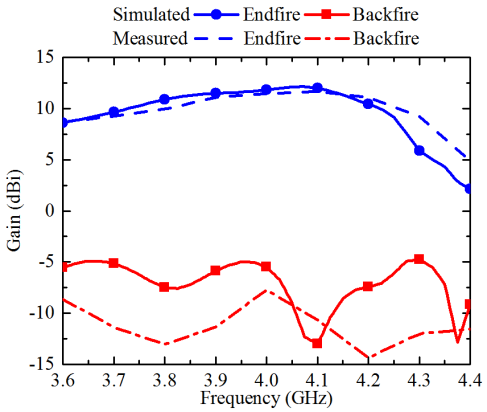


Fig. 12. Simulated and measured endfire gains and backfire gains of the antenna array.

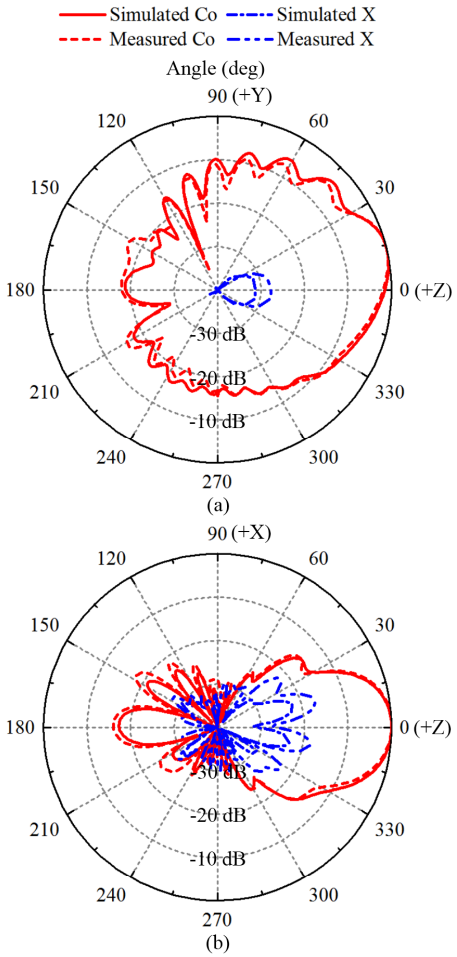


Fig. 13. Simulated and measured normalized radiation patterns of the antenna array on the (a) *YOZ* plane and (b) *XOZ* plane at the center frequency.

32° and 33°, respectively. The slight difference between the simulated and measured results may be attributed to the fabrication and assembly errors.

As shown in Table III, the comparison of the dimension, endfire gain, and gain bandwidth between the existing low-profiled designs in the literature and our design is presented. Designed for wideband applications, the endfire antennas in [3]–[5] have large-gain bandwidths. Nevertheless, owing to the remarkably nonuniform

TABLE III
COMPARISON OF DIMENSIONS AND ENDFIRE GAIN

| Reference | $f_0$ (GHz) | $\varepsilon_r$ | Length ($\lambda_0$) | Width ($\lambda_0$) | Height ($\lambda_0$) | Profile ($\lambda_0$) | Endfire Gain (dBi) | Gain / Length ($1/\sqrt{\lambda_0}$) | -1 dB Gain BW (%) | -3 dB Gain BW (%) |
|---|---|---|---|---|---|---|---|---|---|---|
| [3] | 4.0 | 3.38 | 2.00 | 0.64 | 0.107 | 0.107 | $\approx 1.5$ | $\approx 1.00$ | Large | |
| [4] | 12.0 | 25 | 3.20 | 1.16 | 0.120 | 0.120 | $\approx 2.5$ | $\approx 0.99$ | Large | |
| [5] | 11.0 | 2.2 | 8.54 | 3.67 | 0.330 | 0.019 | $\approx 5.0$ | $\approx 1.08$ | Large | |
| [9] | 5.1 | 2.33 | 2.73 | 1.04 | 0.027 | 0.027 | 7.8 | 3.65 | 3.7 | 7.6 |
| [14] | 5.0 | 1 | 5.98 | 0.38 | 0.018 | 0.018 | 10.8 | 4.92 | 4.0 | 7.0 |
| [15] | 5.0 | 1 | 4.13 | 0.85 | 0.096 | 0.096 | 11.6 | 7.11 | 8.5 | 17.0 |
| Ours | 4.0 | 1 | 3.75 | 0.79 | 0.120 | 0.013 | 11.5 | 7.29 | 9.1 | 17.7 |

aperture distribution, the endfire gains and gain-length ratios of the endfire antennas in [3]–[5] are relatively small compared with the proposed antenna array. The endfire antennas exhibited in [9], [14], and [15] have the characteristics of low profile and high endfire gain. However, due to the partly embedded structure with improved phase constant and aperture distribution, the proposed antenna array has a lower profile and higher gain-length ratio compared with the endfire antennas in [9], [14], and [15]. Moreover, the radiating element of the proposed antenna array has a relatively large dimension with low quality factor, leading to a low fabrication complexity and wide gain bandwidth.

## VI. CONCLUSION

In this communication, an antenna array with low profile and high gain for endfire radiation is presented. The antenna array has a partly embedded structure, a relatively uniform magnitude distribution, and a moderate phase constant. Fabricated only by metal, the proposed antenna array also has the advantages of low cost, light weight, and easy fabrication. With the radiating aperture length of 3.75 $\lambda_0$ and the profile of 0.013 $\lambda_0$, the antenna array obtains a good measured endfire radiation pattern with the endfire gain of 11.5 dBi. The measured 1 and 3 dB gain bandwidths are moderate, which are 9.1% and 17.7%, respectively. The antenna array is a potential candidate for the low-profile long-distance communication applications with the demand of endfire beam with high gain.

## REFERENCES


[1] Z. Hu, Z. Shen, W. Wu, and J. Lu, "Low-profile log-periodic monopole array," *IEEE Trans. Antennas Propag.*, vol. 63, no. 12, pp. 5484–5491, Dec. 2015.

[2] S. Zhang and G. F. Pedersen, "Compact wideband and low-profile antenna mountable on large metallic surfaces," *IEEE Trans. Antennas Propag.*, vol. 65, no. 1, pp. 6–16, Jan. 2017.

[3] Q. Song, Z. Shen, and J. Lu, "Log-periodic monopole array with uniform spacing and uniform height," *IEEE Trans. Antennas Propag.*, vol. 66, no. 9, pp. 4687–4694, Sep. 2018.

[4] Z. Chen and Z. Shen, "Wideband flush-mounted surface wave antenna of very low profile," *IEEE Trans. Antennas Propag.*, vol. 63, no. 6, pp. 2430–2438, Jun. 2015.

[5] P. Wang and Z. Shen, "End-fire surface wave antenna with metasurface coating," *IEEE Access*, vol. 6, pp. 23778–23785, 2018.

[6] Y. Zhao, Z. Shen, and W. Wu, "Wideband and low-profile h-plane ridged SIW horn antenna mounted on a large conducting plane," *IEEE Trans. Antennas Propag.*, vol. 62, no. 11, pp. 5895–5900, Nov. 2014.

[7] Z. Hu, Z. Shen, W. Wu, and J. Lu, "Low-profile top-hat monopole Yagi antenna for end-fire radiation," *IEEE Trans. Antennas Propag.*, vol. 63, no. 7, pp. 2851–2857, Jul. 2015.

[8] Y. Zhao, Z. Shen, and W. Wu, "Wideband and low-profile monocone quasi-Yagi antenna for end-fire radiation," *IEEE Antennas Wireless Propag. Lett.*, vol. 16, pp. 325–328, 2017.

[9] J. Liu and Q. Xue, "Microstrip magnetic dipole Yagi array antenna with endfire radiation and vertical polarization," *IEEE Trans. Antennas Propag.*, vol. 61, no. 3, pp. 1140–1147, Mar. 2013.

[10] J. Liu, D. R. Jackson, and Y. Long, "Substrate integrated waveguide (SIW) leaky-wave antenna with transverse slots," *IEEE Trans. Antennas Propag.*, vol. 60, no. 1, pp. 20–29, Jan. 2012.

[11] J. Liu, D. R. Jackson, Y. Li, C. Zhang, and Y. Long, "Investigations of SIW leaky-wave antenna for endfire-radiation with narrow beam and sidelobe suppression," *IEEE Trans. Antennas Propag.*, vol. 62, no. 9, pp. 4489–4497, Sep. 2014.

[12] Y. Hou, Y. Li, Z. Zhang, and Z. Feng, "Narrow-width periodic leaky-wave antenna array for endfire radiation Based on Hansen–Woodyard condition," *IEEE Trans. Antennas Propag.*, vol. 66, no. 11, pp. 6393–6396, Nov. 2018.

[13] Y. Hou, Y. Li, Z. Zhang, and M. F. Iskander, "Microstrip-fed surface-wave antenna for endfire radiation," *IEEE Trans. Antennas Propag.*, vol. 67, no. 1, pp. 580–584, Jan. 2019.

[14] P. Liu, H. Feng, Y. Li, and Z. Zhang, "Low-profile endfire leaky-wave antenna with air media," *IEEE Trans. Antennas Propag.*, vol. 66, no. 3, pp. 1086–1092, Mar. 2018.

[15] P. Liu, Y. Li, Z. Zhang, and P. Jia, "All-metal centipede-like end-fire antenna," *IEEE Antennas Wireless Propag. Lett.*, vol. 17, no. 10, pp. 1905–1909, Oct. 2018.

[16] D. M. Pozar, *Microwave Engineering*, 4th ed. Hoboken, NJ, USA: Wiley, 2011, ch. 6.

[17] J. L. Volakis, *Antenna Engineering Handbook*, 4th ed. New York, NY, USA: McGraw-Hill, 2007, ch. 11.

[18] Y. Hou, Y. Li, Z. Zhang, and Z. Feng, "A broadband and high-gain endfire antenna array fed by air-substrate parallel strip line," *IEEE Trans. Antennas Propag.*, vol. 67, no. 8, pp. 5717–5722, Aug. 2019.

[19] J. Liu, W. Zhou, and Y. Long, "A simple technique for open-stopband suppression in periodic leaky-wave antennas using two nonidentical elements per unit cell," *IEEE Trans. Antennas Propag.*, vol. 66, no. 6, pp. 2741–2751, Jun. 2018.

[20] W. W. Hansen and J. R. Woodyard, "A new principle in directional antenna design," *Proc. IRE*, vol. 26, no. 3, pp. 333–345, Mar. 1938.

[21] E. M. O'Connor, D. R. Jackson, and S. A. Long, "Extension of the Hansen–Woodyard condition for endfire leaky-wave antennas," *IEEE Antennas Wireless Propag. Lett.*, vol. 9, pp. 1201–1204, 2010.

[22] J. Liu, D. R. Jackson, and Y. Long, "Modal analysis of dielectric-filled rectangular waveguide with transverse slots," *IEEE Trans. Antennas Propagat.*, vol. 59, no. 9, pp. 3194–3203, Sep. 2011.

[23] W. Fuscaldo, D. R. Jackson, and A. Galli, "Beamwidth properties of endfire 1-D leaky-wave antennas," *IEEE Trans. Antennas Propag.*, vol. 65, no. 11, pp. 6120–6125, Nov. 2017.

[24] J. Liu and D. R. Jackson, "Aperture distributions for maximum endfire directivity from a continuous line source with a uniform phase progression," *IEEE Trans. Antennas Propag.*, vol. 65, no. 10, pp. 5123–5136, Oct. 2017.